Journal of Colloid and Interface Science 694 (2025) 137663

Contents lists available at ScienceDirect

Journal of Colloid And Interface Science

journal homepage: www.elsevier.com/locate/jcis

Regular Article

Time-dependent particle size increase during lipid nanoparticle purification by cross-flow filtration

Annabelle Dietrich [1], Nicole Beckert [1], Jürgen Hubbuch [*]

Karlsruhe Institute of Technology (KIT), Institute of Process Engineering in Life Sciences, Section IV: Biomolecular Separation Engineering, Fritz-Haber-Weg 2, Karlsruhe, 76131, Germany

GRAPHICAL ABSTRACT

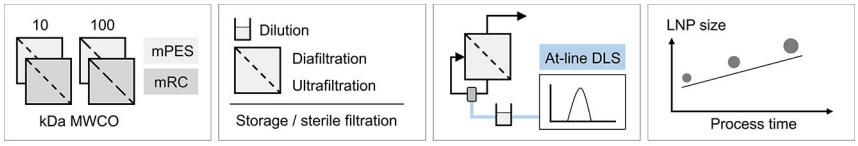

ARTICLE INFO

Keywords:
Lipid nanoparticle
Cross-flow filtration
Particle fusion
Dialysis
At-line monitoring

ABSTRACT

Although cross-flow filtration (CFF) is a time- and resource-efficient purification method, CFF has rarely been explored for lipid nanoparticle (LNP) purification as a scalable alternative to dialysis. CFF-based processing allows for buffer exchange by diafiltration (DF) and setting a target product concentration by ultrafiltration (UF). Herein, we investigate the effect of CFF-based processing on LNP characteristics and process performance by performing a parameter study through the variation of selected membrane-related and operational parameters. We used a pre-dilution approach prior to LNP purification to reduce the ethanol content while maintaining LNP characteristics. Taking advantage of the integration potential of CFF for process analytical technology (PAT), we successfully established size monitoring for LNPs by integrating at-line dynamic light scattering (DLS), providing near real-time process insights. During processing, we observed an increase in LNP size and a change in their size distribution, dependent on processing time but not on the varied process parameters. Following comprehensive off-line analyses, all other LNP characteristics remained constant and final lipid recoveries were achieved in the range of 86–89% for all CFF processes. Long-term, the CFF-purified LNPs showed a lower increase in size compared to the dialyzed LNPs during storage of 14 days. Lastly, examination of purified LNP behavior during sterile filtration revealed changes in particle size in the upper size range. In general, we provide comprehensive insights into CFF-based LNP processing and its impact on LNP characteristics and process performance. Such studies are expected to contribute to the understanding of CFF-based LNP processing and their future application for size-controlled LNP production.

1. Introduction

Lipid nanoparticles (LNPs) as clinically advanced non-viral, lipid-based vector systems have demonstrated significant potential in nucleic acid delivery over the past decade [1,2]. In addition to cationic lipids, which play a key role in nucleic acid encapsulation and release by forming complexes with anionic nucleic acids, LNPs are composed of three other essential components: cholesterol, a phospholipid, and a polyethylene glycol (PEG) lipid, each contributing to the overall functionality of the particle, as reviewed in detail by Albertsen et al. [3]. Next to a de-

* Corresponding author.
E-mail address: juergen.hubbuch@kit.edu (J. Hubbuch).
[1] Contributed equally.

https://doi.org/10.1016/j.jcis.2025.137663
Received 24 February 2025; Received in revised form 16 April 2025; Accepted 20 April 2025

Available online 24 April 2025

sired lipid molar ratio of the aforementioned LNP components, the N/P ratio—representing the balance between cationic lipid amines and nucleic acid phosphate groups—is essential in ensuring efficient nucleic acid encapsulation while maintaining functional stability [4,5]. Overall, achieving a precise LNP composition relies on a controlled LNP synthesis process, while maintaining particle characteristics across further processing requires LNP processing stability.

Using microfluidic mixing devices allows for reproducible and scalable LNP synthesis by mixing the nucleic acid-containing aqueous phase with the lipid-containing organic phase [6]. Here, the mixing parameters total flow rate (TFR) and flow rate ratio (FRR) have been found to have a significant impact on particle size [7,8,5,9]. Nevertheless, the subsequent purification step should not be neglected, as further changes in the physicochemical characteristics of the LNPs have been observed.

Despite its well-known scalability limitations, dialysis is commonly employed to remove the residual organic solvent and adjust the pH to neutrality. Kulkarni et al. [10] and Terada et al. [8] have demonstrated that both solvent removal and pH adjustment contribute concurrently to the particle size increase of LNPs during dialysis.

Pre-treatment approaches prior to dialysis have also been investigated to enhance particle stability. One pre-treatment method involves direct dilution with a buffer solution to reduce the ethanol content. This pre-dilution approach was originally introduced by Jeffs et al. [11], who employed it directly after the mixing step to improve the in-process stability of cationic lipid-containing vesicles. Pre-dilution with low-pH buffer has been later applied to LNPs [12] and further advanced through the development of an integrated microfluidic device designed to rapidly dilute the LNPs under controlled conditions [13]. However, merely diluting the ethanol is insufficient, as a subsequent buffer exchange to physiological pH remains necessary.

Compared to dialysis, cross-flow filtration (CFF) represents a time- and resource-efficient alternative, offering superior scalability and integration potential. CFF operated in constant-volume diafiltration (DF) mode allows for gradual buffer exchange with a DF buffer while maintaining the product volume or in ultrafiltration (UF) mode to concentrate the product to the desired concentration [14]. While only one study has applied CFF for LNP purification [15], other studies have dealt with CFF applications for other related particle types within the broader category of lipid-based particles. The work of Hirsjärvi et al. [16] is among the few that have explicitly compared CFF with dialysis for hybrid lipid-polymer particles.

Unlike diffusion-driven dialysis, pressure-driven CFF requires consideration of operational CFF parameters beyond the membrane-related parameters. However, comprehensive studies on the impact of those parameters on particle characteristics have rarely been reported. Some studies have exclusively explored two types of membrane material [17], molecular weight cut-off (MWCO) [16], or membrane area [18], but no studies have yet investigated those in combination or different membrane formats like hollow fiber or flat sheet. Sakurai et al. [17] has suggested that the hydrophobicity of the membrane is one key factor leading to particle adsorption to the membrane. Typical operational parameters for CFF include feed and filtrate flow rates and the transmembrane pressure (TMP), which is determined by the operating pressures. To date, the reported studies on the variation of those operational parameters cover DF modes other than constant-volume DF, such as single-pass DF [18] and discontinuous DF [19].

Others focused on innovative CFF set-ups, such as in-line DF for continuous processing high in efficiency [20] or a two-step CFF process for improved particle characteristics [15]. Interestingly, Worsham et al. [20] found a permeability limitation of the membrane caused by the initial exposure to ethanol, suggesting a pre-dilution strategy to significantly reduce the amount of DF stages. Efforts to improve scalability have driven the development of a miniaturized, on-chip CFF purification system that enables synthesis and purification on a micro-volume scale [19]. Alongside scalability, another area of innovation lies in integrating real-time measurement of particle characteristics, building on

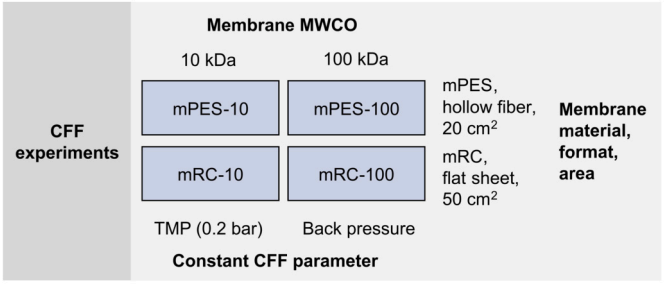

Fig. 1. Illustration of membrane characteristics and operational filtration parameters for the four CFF experiments performed. Abbreviations: CFF: cross-flow filtration, mPES: modified polyethersulfone, mRC: modified regenerated cellulose, MWCO: molecular weight cut-off, TMP: transmembrane pressure.

the process analytical technology (PAT) framework introduced by the FDA [21]. While measuring particle characteristics between process steps is common practice, at-line measurements [22] remain relatively rare. Significant progress has been made in using sensors for real-time process monitoring, allowing for time-resolved insights within a single process step [23]. However, particle size measurements of LNPs during the constant-volume DF process have so far only been conducted off-line [15], with at-line monitoring still not achieved.

Thus far, comprehensive insights into CFF-based LNP processing have not been reported, nor have CFF parameter variations and their impact on LNP characteristics been considered.

In this study, we investigate the impact of membrane-related and operational CFF parameters on process performance and LNP characteristics during LNP purification by CFF. To estimate the effect of dilution with low-pH buffer as a pretreatment procedure on LNP characteristics, we initially performed dialysis experiments with pre- and undiluted LNPs. The pre-diluted LNPs also served as the starting material for the CFF experiments, making the dialysis experiments a direct reference for the corresponding CFF processes. To address time- and resource-efficient buffer exchange and product concentration, we applied CFF with constant-volume DF mode over six diafiltration volumes (DVs) followed by concentration of LNPs using the UF mode. Across the CFF experiments, we varied either the membrane characteristics material, format, and area, or the membrane MWCO and the system pressure setting, as schematically illustrated in Fig. 1. Further, we established at-line dynamic light scattering (DLS) measurements to gain time-resolved insights into changes in particle size and size distribution in near real-time, also emphasizing the potential to integrate PAT tools into CFF set-ups for process monitoring. Subsequently, LNP samples taken between process steps and at various points throughout the CFF process were subjected to thorough stability assessment over a 14-day storage period and evaluated regarding particle size, surface charge, encapsulation efficiency, as well as lipid concentration, molar ratio, and recovery. Lastly, the effect of sterile filtration on particle size, size distribution, and lipid recovery was investigated.

2. Materials and methods

2.1. Materials, buffers, and solvents

Unless otherwise specified, chemicals were obtained from Merck (Darmstadt, Germany). The lipids 1,2-Dioleoyl-3-trimethylammonium-propane (chloride salt) (DOTAP) and 1,2-Dioctadecanoyl-sn-glycero-3-phosphocholin (DSPC), kindly provided by Lipoid (Ludwigshafen, Germany), were used alongside 1,2-Dimyristoyl-rac-glycero-3-methoxy-polyethylene glycol-2000 (DMG-PEG) purchased from Avanti Polar Lipids (Alabaster, AL, USA) and cholesterol. Ultrapure water (Purelab ultra, ELGA LabWater, High Wycombe, UK), sodium acetate trihydrate, acetic acid, and tris(hydroxymethyl)aminomethane (tris) were used for the preparation of acetate (25 mM, pH 4.0) and tris (10 mM,

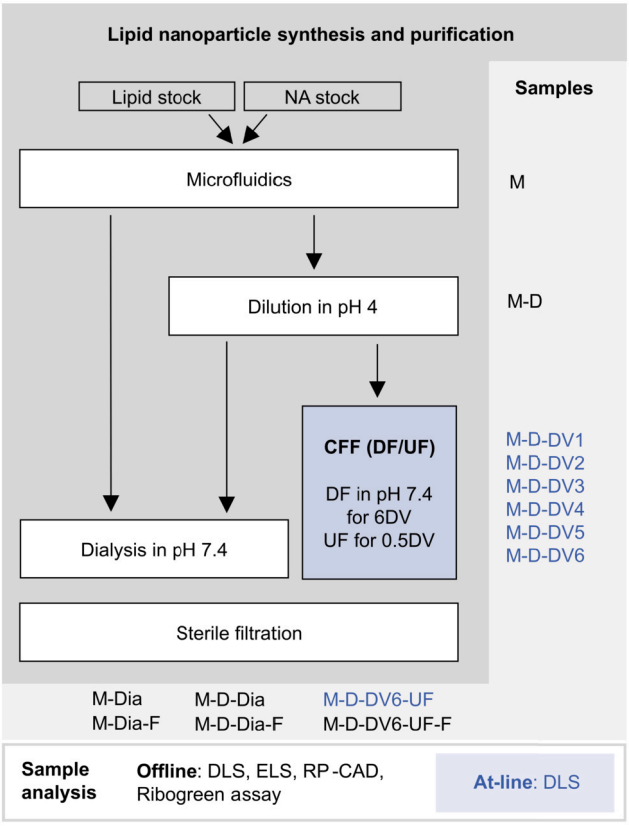

Fig. 2. Workflow illustration of sequential process steps for LNP synthesis and purification, sampling, and sample analysis. At-line DLS was performed for CFF intermediates and final CFF-purified LNPs. Abbreviations: CAD: charged aerosol detection, CFF: cross-flow filtration, D: dilution, DF: diafiltration, Dia: dialysis, DLS: dynamic light scattering, DV: DF volume, ELS: electrophoretic light scattering, F: sterile filtration, M: microfluidics, NA: nucleic acid, RP: reversed-phase, UF: ultrafiltration. (For interpretation of the colors in the figure(s), the reader is referred to the web version of this article.)

pH 7.4) buffers. A SenTix62 pH electrode (WTW, Weilheim, Germany) combined with a HI 3220 pH meter (Hanna Instruments, Woonsocket, RI, USA) was employed for pH adjustments of the buffers using hydrochloric acid solution (32%), followed by sterile filtration through 0.2 µm cellulose acetate filters (VWR International, Radnor, PA, USA). For high performance liquid chromatography (HPLC), water and acetonitril (ACN) containing 0.1% trifluoroacetic acid (TFA) (v/v) were obtained in LC-MS grade from Thermo Fisher Scientific Inc. (Waltham, MA, USA), LC-MS grade ACN was purchased from VWR Chemicals (VWR International) and HPLC grade ethanol was used. Primers (forward: 5'-ATGGTGAGCAAGGGCGAGTT-3', reverse: 5'-CTCGCCCTTGCTCACCATTT-3'), Quant-iT™ RiboGreen™ Assay Kit, NoLimits™ 20 bp DNA fragments, Triton™ X-100, and 384-well Nunclon™ Delta Surface microplates were purchased from Thermo Fisher Scientific Inc.

2.2. Lipid nanoparticle synthesis and purification

The sequential process steps for lipid nanoparticle synthesis and purification are illustrated in Fig. 2.

The aqueous nucleic acid stock solution with a concentration of 119 µg mL^{-1} in acetate buffer was prepared according to Beckert et al. [24]. For the lipid stock solution with a total lipid concentration of 12 mg mL^{-1}, DOTAP, DSPC, DMG-PEG, and cholesterol (50:10:38.5:1.5 mol%) were dissolved in ethanol using a Branson Ultrasonics sonifier SFX550 (Thermo Fisher Scientific Inc.). Glass syringes in 10 mL (SETsonic GmbH, Ilmenau, Germany) and 1 mL (Innovative Labor Systeme GmbH, Stützerbach, Germany) scales were filled with nucleic acid and lipid stock solutions, respectively, and clamped into a Nemesys pump (Cetoni GmbH, Korbußen, Germany). LNPs with an N/P ratio of 5 were synthesized in a connected herringbone-structured microfluidic chip (Microfluidic ChipShop, Jena, Germany) at a FRR of 5:1 (aqueous:organic) and a TFR of 20 mL min^{-1}.

Synthesized LNPs by microfluidics (M) were either used directly or further pre-diluted 1:4 (M-D) with pH 4 acetate buffer to reduce the ethanol content. Subsequent purification was performed by dialysis or CFF using pH 7.4 tris buffer.

For reference, both synthesized and pre-diluted LNPs were further dialyzed (M-Dia and M-D-Dia) using 10 kDa Slide-A-Lyzer® dialysis cassettes (1–3 mL, regenerated cellulose, Thermo Fisher Scientific Inc.). The dialysis process involved at least 500 volumes of buffer relative to the sample and was carried out at 2–8 °C for 4 h and overnight.

For purification by CFF, a KrosFlo Research KRIIi CFF system equipped with an automatic back pressure valve (Spectrum Labs, Rancho Dominguez, CA, USA), a stirred 50 mL reservoir (Sartorius Stedim Biotech GmbH, Göttingen, Germany), and an Ohaus® Scout® Pro balance (Ohaus, Parsippany, NJ, USA) was used. The filter modules used differ in MWCO (10 kDa and 100 kDa) as well as in the membrane's characteristics material, format, and area: modified polyethersulfone (mPES) hollow fiber filter modules with 20 cm^2 (Spectrum® MicroKros, Repligen, Waltham, MA, USA) and modified regenerated cellulose (mRC) flat sheet filter modules with 50 cm^2 (Hydrosart®, Sartocon® Slice 50, Sartorius). It has to be noted that the shear rates induced by the membrane vary between the two membrane formats but are independent of the MWCO. With each filter module, one DF/UF process was performed at room temperature with a constant feed flow rate of 15 mL min^{-1}, which represents a consistent shear rate induced by the pump. For simplicity, the CFF experiments are named based on the combination of membrane material and MWCO in kDa: mPES-10, mPES-100, mRC-10, mRC-100. Aiming for a processing time within fifty to seventy minutes, the CFF set-ups were adjusted by setting required pressures to account for MWCO-related differences in membrane permeability. The TMP was set to 0.2 bar for both processes with the 10 kDa membranes (mPES-10, mRC-10) to increase the permeate flux, whereas for the ones with the 100 kDa membranes (mPES-100, mRC-100) a permeate capillary smaller in diameter adjusted the back pressure to restrict the permeate flux. Constant-volume DF (12 mL DV) was conducted with pre-diluted LNPs exchanging six DV. The retentate was sampled through an injection plug (Fresenius Kabi, Bad Homburg, Germany) every DV (M-D-DV[1-6]). By decoupling the DF buffer, LNPs were subsequently concentrated twofold by UF (M-D-DV6-UF).

All CFF-derived samples were immediately analyzed by at-line DLS. All samples were stored at 2–8 °C and analyzed off-line by DLS, electrophoretic light scattering (ELS), reversed-phase (RP)-charged aerosol detection (CAD), and a fluorescence-based assay after 1, 7, and 14 days. After 7 days, 400 µL of the final samples derived from dialysis and CFF processes were manually sterile-filtered through 0.22 µm, 0.1 cm^2 Millex® polyvinylidene fluoride syringe filters (M-Dia-F, M-D-Dia-F, M-D-DV6-UF-F), which corresponds to 40 L m^{-2}, and analyzed.

Supplementary dialysis experiments with pre-diluted and undiluted LNP solution were executed as described in Appendix A.1.1.

2.3. Analytics

2.3.1. Light scattering

Light scattering techniques were employed to monitor particle size and surface charge. DLS was used to measure at-line and off-line particle sizes. Measurements were performed using a Zetasizer Nano ZSP with the Zetasizer software version 7.12 (Malvern Instruments Ltd., Malvern, UK). Measurements were performed in a low-volume quartz cuvette (ZEN2112, Malvern Panalytical Ltd., Malvern, UK) and with a laser beam focused at a wavelength of 633 nm with an attenuation of 5. Scattering was detected at an angle of 173°. The refractive index (RI)

of the LNPs was set to 1.333 with an absorption value of 0.01, while the dispersant had a RI of 1.341 and a viscosity of 1.919 cP. Samples derived from processes without the dilution step (M, M-Dia, M-Dia-F) were diluted to a lipid concentration of 0.5 mg mL^{-1}, while all other samples were measured directly. Duplicate measurements were performed using automatic measurement durations, with two sub-measurements for at-line samples and three sub-measurements for off-line samples.

Using the same device and software, ELS was performed to assess the surface charge of the LNPs. Measurements were carried out using a folded capillary cell (DTS1070, Malvern Panalytical Ltd.). A dielectric constant (ε_r) of 78.5 was applied, and the Helmholtz–Smoluchowski equation was used for calculations. Samples were measured directly except for those from processes without the dilution step (M, M-Dia, M-Dia-F), which were set to a total lipid concentration of 1 mg mL^{-1}. Each sample was measured in duplicate at 60 V, with two sub-measurements interrupted by a 120 s delay.

2.3.2. Reversed phase - charged aerosol detection

Lipid concentration and molar ratio were analyzed using the previously developed and calibrated RP-CAD method by Beckert et al. [24]. In brief, a 2.1 × 150 mm ACQUITY® BEH Phenyl column (1.7 µm particle size, 130 Å pore size, Waters, Milford, CT, USA) was employed alongside a VanGuard™ pre-column (2.1 × 5 mm). The column was connected to a 3000 RS HPLC system (Dionex Corporation, Sunnyvale, CA, USA) equipped with a 3000 RS diode array detector and a Corona Veo CAD RS, all operated via Chromeleon 6.8 software (Thermo Fisher Scientific Inc.). The column and autosampler temperatures were set to 50 °C and 8 °C, respectively. CAD settings comprised a 35 °C evaporation temperature, a 3.6 s filter constant, and a power function value of 1.3. Under a flow rate of 0.3 mL min^{-1}, with 0.1% TFA (v/v) in water as mobile phase A and 0.1% TFA (v/v) in ACN as mobile phase B, the method started at 40% B for 4 min, followed by two linear gradients to 70% B (1 min) and 100% B (11.25 min). After 2 min at 100% B, a one-minute gradient was applied to return to initial conditions. Samples were diluted with ethanol to achieve final concentrations corresponding to those within the calibration curves and measured in duplicate using an 8 µL injection volume. The total lipid concentrations prior to and after the process steps dialysis and CFF and the volume were used for lipid recovery calculations.

2.3.3. Fluorescence-based assay

Nucleic acid encapsulation was determined using the fluorescence-based assay kit Quant-iT™ RiboGreen™. Samples were analyzed according to the manufacturer's protocol, with the following modifications: NoLimits™ 20 bp DNA fragments were used for reference measurement with and without 1% Triton™ X-100. Samples were diluted and treated with dye in both conditions. Samples were prepared in duplicate, 384-well black polystyrene microplates were used, and fluorescence was measured ($\lambda_{ex} = 480$ nm, $\lambda_{em} = 520$ nm) with a Spark® microplate reader (Tecan Group Ltd., Männedorf, CH). The encapsulation efficiency (EE), defined as the proportion of nucleic acids encapsulated within LNPs, was determined using equation (1):

$$EE = \frac{f_{total} - f_{free}}{f_{total}} * 100\%. \quad (1)$$

Here, f_{total} denotes the blank-corrected fluorescence of nucleic acids in the sample after treatment with Triton™ X-100 and f_{free} represents the blank-corrected fluorescence of the unencapsulated nucleic acids located outside the LNPs.

2.3.4. Statistical evaluation

MATLAB® R2021a (The MathWorks Inc., Natick, MA, USA) was used for data analysis and visualization. Replicate measurements are reported as the mean ± standard deviation.

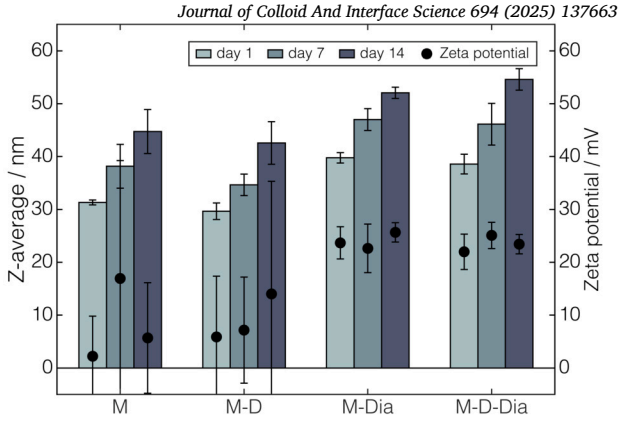

Fig. 3. Effects of dilution as a pre-treatment step prior to dialysis on LNP Z-average and zeta potential. The procedure of LNP synthesis, pre-dilution, dialysis, and storage at 2–8 °C for up to 14 days was carried out four times (n = 4) and samples were measured in duplicates (m = 2). Abbreviations: D: dilution, Dia: dialysis, LNP: lipid nanoparticle, M: microfluidics.

3. Results

3.1. Reduction of ethanol content by dilution

To evaluate a potential stabilizing effect of dilution with pH 4 buffer as a pre-treatment procedure prior to dialysis into pH 7.4 buffer, LNPs were synthesized, dialyzed either undiluted or pre-diluted (cf. Fig. 2), and stored at 2–8 °C. Fig. 3 illustrates changes in the Z-average and zeta potential values of LNPs across those different process stages.

Post-synthesis by microfluidics, particle sizes of undiluted (M) and pre-diluted (M-D) LNPs were within the same range. While dialysis led to an overall size increase, no substantial differences were observed between directly dialyzed (M-Dia) and pre-diluted (M-D-Dia) LNPs. Similarly, consistent size increases over time were observed for synthesized or dialyzed LNPs, regardless of whether they were un- or pre-diluted. Zeta potential measurements exhibit significant variability for synthesized LNPs, while a consistent surface charge of 20 to 25 mV was observed for dialyzed LNPs.

The effect of the surrounding solution composition on zeta potential measurements was assessed by an additional dialysis experiment into pH 4 buffer (cf. Supplementary Figure A.1). Stable zeta potential measurements were observed for LNPs present in pH 4 buffer after the removal of ethanol (cf. Supplementary Figure A.2).

The effect of the dialysis buffer pH on the size increase during dialysis was further evaluated by step-wise dialysis in an additional dialysis experiment (cf. Supplementary Figure A.1). The two-step dialysis allows for the initial removal of ethanol, followed by a subsequent adjustment to physiological pH. Regardless of the pre-dilution, dialysis into pH 4 buffer led to a size increase, further enhanced upon subsequent dialysis into pH 7.4 buffer, eventually reaching a comparable size as observed with direct dialysis into pH 7.4 buffer (cf. Supplementary Figure A.2). Further, a similar increase in particle size was observed over the storage period for direct or two-step dialyzed LNPs.

In summary, dilution with pH 4 buffer after LNP synthesis reduces the ethanol content of the surrounding solution, but neither stabilizing nor destabilizing effects on the particle size were observed.

3.2. Cross-flow filtration—flow and pressure characteristics

Membrane-related and operational CFF parameters were varied in a process parameter study to investigate their impact on LNP characteristics during LNP purification by CFF. The four CFF experiments systematically differed in membrane MWCO and pressure setting as well as membrane material, format, and area (cf. Fig. 1).

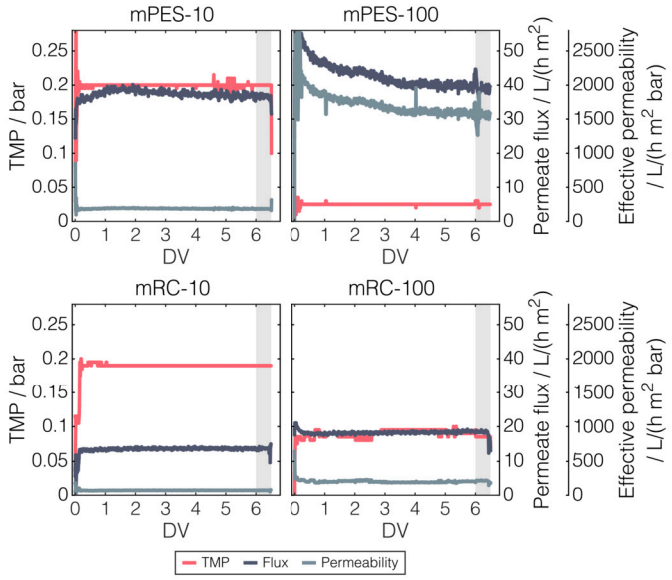

Fig. 4. Profiles of TMP, permeate flux, and effective permeability during CFF-based processing. CFF experiments were performed with mPES-10 (a), mPES-100 (b), mRC-10 (c), and mRC-100 (d) membranes in DF/UF mode with UF highlighted with shaded bars. Abbreviations: CFF: cross-flow filtration, DF: diafiltration, DV: diafiltration volume, mPES: modified polyethersulfone, mRC: modified regenerated cellulose, TMP: transmembrane pressure, UF: ultrafiltration.

Fig. 4 illustrates changes in the monitored TMP, permeate flux, and effective permeability throughout CFF-based DF for buffer exchange and UF for product concentration.

Comparing the runs using 10 kDa MWCO membranes under constant TMP, a higher permeate flux was observed for the mPES than mRC membrane (cf. Fig. 4 (a), (c)), which might be attributed to the membrane material and format. A similar observation occurred during the runs with 100 kDa MWCO membranes under constant permeate back pressure (cf. Fig. 4 (b), (d)). Comparing those runs under constant permeate back pressure, a three-times lower TMP was observed for the mPES than mRC membrane, which may be linked to the membrane format and area. Interestingly, changes in the permeate fluxes were observed for 100 kDa MWCO membranes under constant permeate back pressure, with a pronounced decrease for mPES-100 throughout the entire process compared to a rather moderate drop for mRC-100 during the first 0.5 DV (cf. Fig. 4 (b), (d)). However, the TMP remained constant in both cases.

Through the effective permeability, which relates the permeate flux to the TMP, it can be derived that the membrane material and format—mPES hollow fiber filter modules are generally more permeable than mRC flat sheet filter modules—as well as the MWCO—larger MWCO are more permeable—affect the CFF process. Lower TMPs and higher permeate fluxes were observed for the 100 kDa than the 10 kDa MWCO membranes, which is further attributed to the MWCO-related pressure control applied in the respective CFF set-ups.

Overall, no difference in terms of pressure or permeate flux was observed in either of the processes regarding the two CFF-based processing modes—DF for buffer exchange and UF for concentration. In summary, the observed profiles of the TMP, permeate flux, and effective permeability throughout processing can be linked to the membrane-related and operational CFF parameters.

3.3. Cross-flow filtration—lipid nanoparticle characteristics

Throughout LNP purification by CFF, the Z-average was directly measured at-line for every DV and supplemented with off-line data from day 1, as shown in Fig. 5.

The increase in LNP particle size represents the key finding throughout processing by CFF. Final Z-average values ranging between 90 to 116 nm were observed by at-line DLS after DF for six DV and UF, representing a substantially higher increase in particle size compared to those purified by dialysis (cf. Fig. 5 (a)–(d)). With an increase of approximately 10 nm, the final Z-average values of dialyzed LNPs were less than 50% of those measured for the DF/UF-purified LNPs.

The comparison of at-line and off-line DLS measurements reveals a consistent pattern in particle size. For CFF-purified LNPs from the third or fourth DV onward, Z-average values from at-line DLS analyses consistently exceed those obtained from off-line analyses on day 1 (cf. Fig. 5 (a)–(d)). It has to be noted that the at-line DLS measurements confirm the Z-average increase observed in the off-line data, which highlights DLS as a suitable at-line monitoring tool.

The increase in Z-average occurred proportionally with the number of DVs, with noticeable differences between each of the four CFF runs, as shown in Fig. 5 (e). Starting from the measurement at the first DV, the CFF run with the mRC-10 membrane consistently produced the largest LNPs, with progressively smaller LNPs observed in the order of mPES-10, mPES-100, and mRC-100. Overall, the increase in particle size seems independent of the varied membrane-related and operational CFF parameters as well as the DV.

However, the illustration of the Z-average over the processing time exhibits a clear trend (cf. Fig. 5 (f)) of the time-dependent increase in particle size. Differences in membrane characteristics or applied operational CFF parameters appear to influence LNP size primarily through their effect on processing time. Consequently, the lower the permeate flow rate, the longer the processing time, resulting in larger final particle sizes.

Generally, the Z-average is derived from the intensity-weighted size distribution. The progression of the change in the intensity-weighted size distribution throughout the CFF is exemplarily shown for mPES-10 in Fig. 6, with the Z-average values for the starting material (M-D) and the final CFF-purified LNPs (M-D-DV6-UF) indicated by vertical lines.

Initially starting from a mono-disperse distribution, a second population is observed that increases in intensity throughout the CFF. Similar trends were observed for the other CFF runs (cf. Supplementary Figure A.3), with a more or less pronounced second population or overlap between the two populations. It has to be noted that the formation of a second population could not be observed for purification by dialysis (data not shown). Instead, only a shift of the mono-disperse distribution along the X-axis compared to the starting material was observed, which explains the increase in the Z-average.

Along with the Z-average and size distribution, a trend throughout CFF-based processing can also be observed for the zeta potential (cf. Fig. 5 (a)–(d)). For synthesized, diluted LNPs containing 4.17% ethanol (M-D), which served as the starting material for the CFF, the zeta potential values are around zero but exhibit large standard deviations. As the CFF processing progresses, the zeta potential increases, eventually reaching a plateau after four DVs (M-D-DV4). Prior to reaching this plateau, larger standard deviations of the zeta potential measurements were observed, which can be attributed to the presence of ethanol (cf. Section 3.1). Overall, the surface charge profile of LNPs indicates the progression of buffer exchange throughout CFF-based processing.

Throughout LNP purification by CFF, lipid concentration, molar ratio, and recovery were determined every DV by RP-CAD to complement LNP characteristics and evaluate the process performance. Fig. 7 illustrates changes in total lipid concentration and recovery for all four CFF processes across processing. Similar trends were observed for all four processes. The total lipid concentration decreased with each DV, which can be attributed to the sampling procedure. Here, one-twelfth of the process volume is sampled every DV and automatically replaced by the DF buffer due to constant-volume DF mode. By UF-based product concentration, the initial concentration (M-D) was again reached or exceeded. No changes in the lipid molar ratio could be observed (cf. Supplementary Figure A.4). Further, final recoveries ranging from

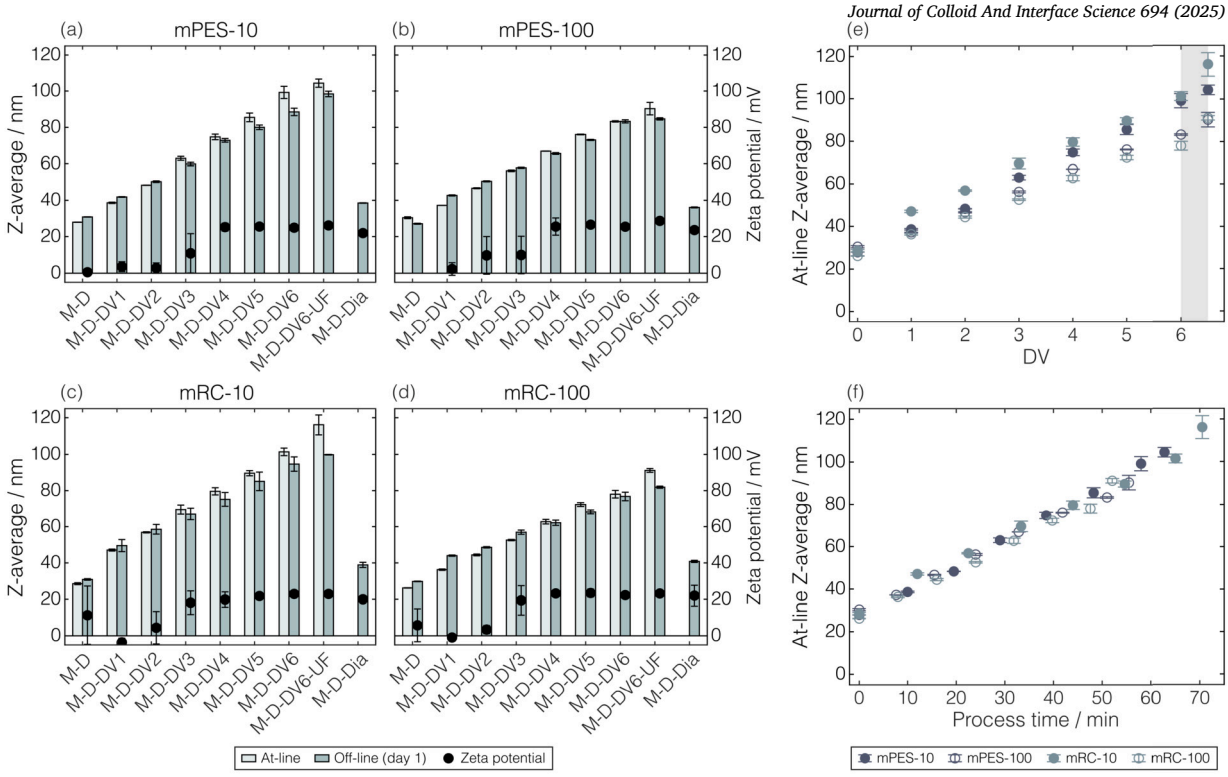

Fig. 5. Changes in Z-average of LNPs across processing. Z-average values for at-line and off-line measurements are illustrated for mPES-10 (a), mPES-100 (b), mRC-10 (c), and mRC-100 (d) membranes with the corresponding zeta potential values. For each membrane, the at-line derived Z-average is shown over DV with UF highlighted by a shaded bar (e) and over processing time (f). Abbreviations: D: dilution, Dia: dialysis, DV: diafiltration volume, M: microfluidics, mPES: modified polyethersulfone, mRC: modified regenerated cellulose, LNP: lipid nanoparticle, UF: ultrafiltration.

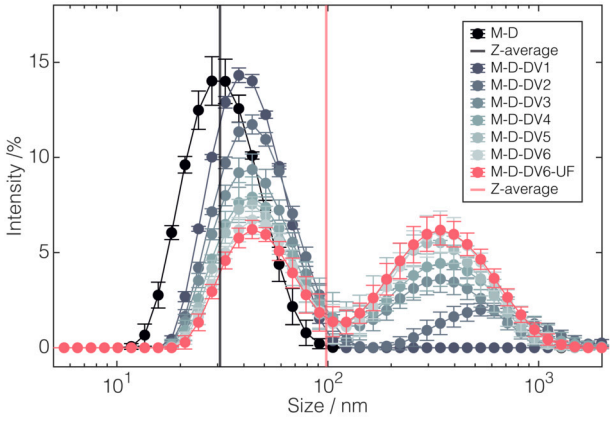

Fig. 6. Changes in the intensity-weighted size distribution for mPES-10. Next to the shown intensity-weighted size distributions for the CFF intermediates of the mPES-10 CFF run, the Z-average values for the synthesized, diluted LNPs (M-D), which served as the starting material for the CFF, and the final CFF-purified LNPs (M-D-DV6-UF) are marked by vertical lines. Abbreviations: CFF: cross-flow filtration, D: dilution, Dia: dialysis, DV: diafiltration volume, LNP: lipid nanoparticle, mPES: modified polyethersulfone, UF: ultrafiltration.

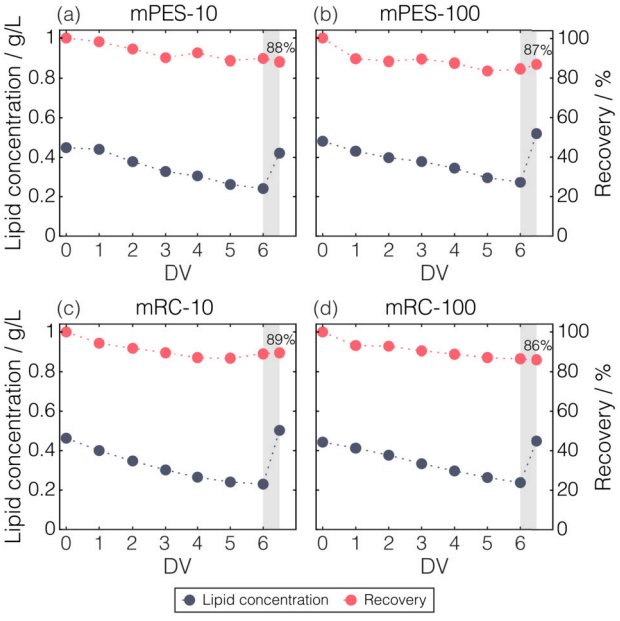

Fig. 7. Changes in total lipid concentration and recovery across processing. RP-CAD-derived total lipid concentration and percentage recovery are illustrated for the CFF runs with mPES-10 (a), mPES-100 (b), mRC-10 (c), and mRC-100 (d) membranes. UF is highlighted by shaded bars. Abbreviations: CAD: charged aerosol detection, CFF: cross-flow filtration, DV: diafiltration volume, mPES: modified polyethersulfone, mRC: modified regenerated cellulose, RP: reversed-phase, UF: ultrafiltration.

86% to 89% were achieved, reflecting the overall performance of CFF processes in such small scales. Although dialysis experiments yielded higher recoveries ranging from 89% to 99%, notable dilution effects were observed with dilution factors between 1.3 and 1.5. The encapsulation efficiencies are comparable across all experiments and remained constant throughout the process, regardless of whether the LNPs were pre-diluted, dialyzed, or purified by CFF.

In summary, both at-line and off-line measurements showed a similar trend of increasing z-average values across CFF-based processing. Here, intensity-based size distributions revealed the appearance of a second population, with a continuous increase in its proportion. Overall, LNP particle size is primarily influenced by the effect of applied CFF settings on total processing time.

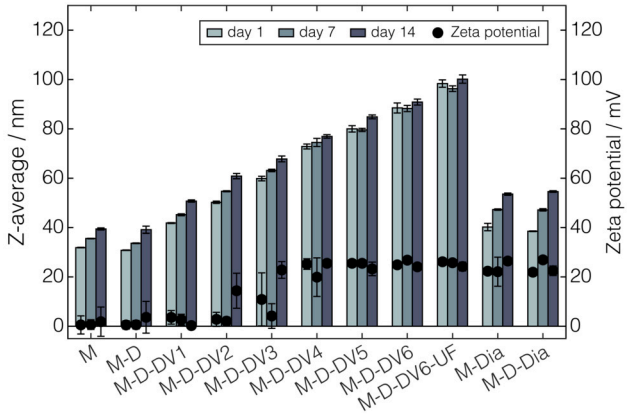

Fig. 8. Changes in Z-average and zeta potential during storage. Z-average and zeta potential values during the storage of 14 days at 2–8 °C are shown for LNPs processed by dialysis or CFF using a mPES-10 membrane. Abbreviations: CFF: cross-flow filtration, D: dilution, Dia: dialysis, DV: diafiltration volume, LNP: lipid nanoparticle, M: microfluidics, mPES: modified polyethersulfone, UF: ultrafiltration.

3.4. Storage stability

LNPs were subjected to a short-time storage stability examination at 2–8 °C for up to 14 days. Changes in Z-average and zeta potential at all processing states are depicted for mPES-10 in Fig. 8.

Over storage, the Z-average of LNPs increased slightly. Interestingly, the Z-average increase during storage was more pronounced for dialyzed LNPs compared to LNPs purified by CFF. Similar trends were observed for the other CFF runs (cf. Supplementary Figure A.5). Dialyzed LNPs showed mono-disperse size distributions during storage (data not shown).

Along with the zeta potential remaining constant (cf. Supplementary Figure A.5), no changes were observed in the other LNP characteristics of lipid concentration, lipid molar ratio, and encapsulation efficiencies throughout the storage period (data not shown). In summary, a more pronounced particle size increase over the storage period was found for the dialyzed LNPs compared to the CFF-purified LNPs.

3.5. Sterile filtration

Filter experiments were conducted after dialysis and CFF to assess the impact of sterile filtration on the removal of larger particles. CFF in DF-UF mode led to the formation of a second, larger-sized LNP population (cf. Fig. 6), resulting in larger Z-average values for CFF-purified LNPs compared to dialyzed LNPs (cf. Fig. 5). Fig. 9 illustrates the intensity-weighted size distribution for CFF-purified LNPs (M-D-DV6-UF) and further sterile filtered LNPs (M-D-DV6-UF-F) for all performed CFF experiments.

Through sterile filtration of CFF-purified LNPs, the presence of intermediate-sized species increased, the Z-average decreased, and recoveries ranged between 73% and 91% (cf. Table 1). Sterile filtration of the CFF-purified LNPs by mRC-10, which showed the largest Z-average and rather broad size distribution, resulted in an overall Z-average reduction of 5 nm and clearance of the larger LNP population at 1000 nm. It has to be noted that no particles larger than 1000 nm were observed in any of the other systems either. These intensity-weighted size distributions still exhibit a more or less pronounced second population, which can be attributed to the size distribution before sterile filtration.

On the contrary, no substantial changes in size distribution, and therefore in Z-average, were observed after sterile filtration of dialyzed LNPs. Generally, lower lipid recoveries were found after sterile filtration of pre-diluted (M-D-Dia-F) than undiluted, dialyzed LNPs (M-Dia-F) (cf. Table 1), indicating a concentration dependency.

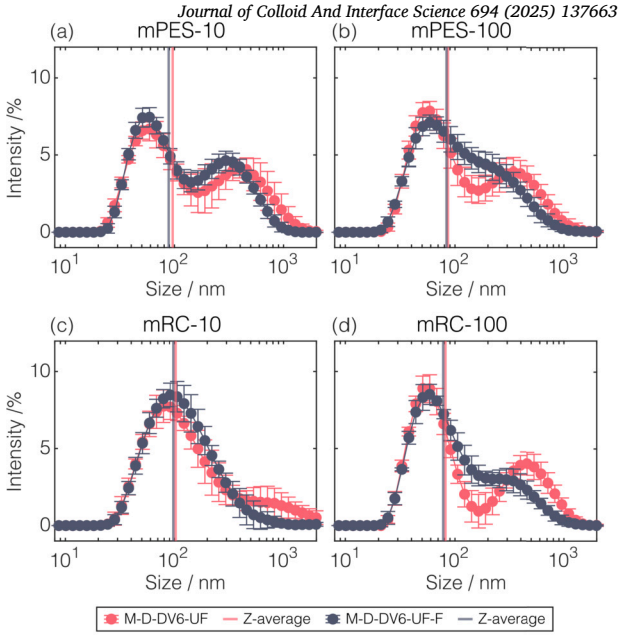

Fig. 9. Intensity-weighted size distribution for CFF-purified and sterile-filtered LNPs. Next to the size distributions, the Z-average values for the CFF-purified (M-D-DV6-UF) and further sterile filtered LNPs (M-D-DV6-UF-F) are marked by vertical lines. Abbreviations: CFF: cross-flow filtration, D: dilution, DV: diafiltration volume, F: sterile filtration, LNP: lipid nanoparticle, M: microfluidics, mPES: modified polyethersulfone, mRC: modified regenerated cellulose, UF: ultrafiltration.

Table 1
Lipid recoveries after sterile filtration. The percentage lipid recoveries of sterile-filtered LNPs after purification by CFF or dialysis are listed. Abbreviations: CFF: cross-flow filtration, D: dilution, Dia: dialysis, DV: diafiltration volume, F: sterile filtration, LNP: lipid nanoparticle, M: microfluidics, mPES: modified polyethersulfone, mRC: modified regenerated cellulose, UF: ultrafiltration.

	Recovery / %			
	mPES-100	mPES-10	mRC-100	mRC-10
M-D-DV6-UF-F	91	72	83	91
M-Dia-F	n.d.	87	96	96
M-D-Dia-F	76	74	89	79

In summary, sterile filtration of LNPs introduced changes in the particle size distribution in the larger size range, resulting in a higher proportion of intermediate-sized particles.

4. Discussion

4.1. Effects of pre-dilution prior to purification by dialysis

Initially, a series of dialysis experiments was conducted with pre-diluted and undiluted LNPs to assess the impact of pre-dilution with a low-pH buffer as a pre-treatment step on LNP characteristics.

In general, pre-dilution was reported to improve particle characteristics of lipid-based particles. Jeffs et al. [11] observed enhanced process stability and higher encapsulation efficiencies for cationic, lipid-containing vesicles, while Kimura et al. [13] specifically identified a slight decrease in particle size for LNPs. Although we did not observe any of those changes in LNP characteristics due to pre-dilution, it is worth noting that the LNPs showed stable behavior.

As LNP dilution with a buffer reduces the ethanol content, related changes in particle characteristics may be linked to the altered behavior of lipids. Ethanol interacts with the polar head groups of lipids at the lipid-water interface due to its dual lipophilic and hydrophilic nature.

In the case of lipid bilayers, this ethanol-lipid interaction expands the membrane surface, creating cavities within the hydrophobic core, which are subsequently occupied by lipid tails from the opposing membrane leaflet, leading to a reduction in membrane thickness [25,26]. Next to this so-called interdigitation process, ethanol-lipid interactions might also enhance the likelihood of fusion due to reduced lipid hybridization and enhanced exposure of lipid tails [27]. Their study also demonstrated increased fusion activity for liposomes with non-protein-containing lipid bilayers next to elevated membrane fluidity. So far, fusion processes in the presence of ethanol have only been studied in the context of liposomes fusing to model bilayer membranes, but to the best of the authors' knowledge, neither studied for LNPs fusing to model bilayer membranes nor LNP-LNP fusion.

The dilution process design for LNPs is rarely reported in the literature. Next to dilution by simple pipetting, Kimura et al. [13] designed a microfluidic on-device dilution system integrating dilution next to LNP synthesis. Compared to pipette-induced dilution or direct dialysis, their rapid dilution approach yielded smaller LNPs, with the smallest particles observed at the highest dilution flow rates. They also hypothesized that ethanol dilution within milliseconds prevents the formation of interdigitated structures and particle fusion. Reducing the ethanol content immediately after LNP synthesis is further supported by molecular dynamics simulations [28] and the observations that longer hold times before dilution [13] or dialysis [29] led to an increase in particle size. So far, no studies on buffer selection for pre-dilution of LNPs have been reported. The authors ultimately chose the synthesis buffer as the dilution buffer, which has also been used for liposomes [30]. However, others selected a dilution buffer pH of 6 for LNPs, which fell between the pH of the synthesis and dialysis buffers [13]. In contrast to the effect of buffer selection for pre-dilution of LNPs, the impact of buffer pH during dialysis on the size increase of LNPs has already been studied [10,8].

In summary, pre-dilution with pH 4 buffer specifically reduced the ethanol content without altering the LNP characteristics, making it suitable for use as a pre-treatment for LNPs prior to CFF-based purification.

4.2. Design of cross-flow filtration-based processing

A CFF-based process in DF/UF mode allows for setting a target product concentration directly after buffer exchange, which is not possible with dialysis. In such filtration-based processes, it is crucial to consider membrane-related and operational parameters, their relationship, and their interaction with or influence on the target product to be filtered.

As ethanol is known to influence the permeability of membranes, LNPs were pre-diluted to lower the ethanol content by a factor of four. Although some studies on liposomes incorporated ethanol dilution prior to constant-volume DF [31,32] or continuous in-line DF [33,20] resulting in increased efficiency [20], this approach has not yet been applied to LNPs. An ethanol-dependent limited permeability of the membrane at the beginning of the process would be reflected by either a lower permeate flux under constant TMP (mPES-/mRC-10) or a higher TMP under constant permeate back-pressure (mPES-/mRC-100) compared to the following process profiles, which, however, could not be observed in our CFF runs.

In the design of filtration processes, membrane-related parameters influence the configuration of operational parameters, which, unlike in diffusion-driven dialysis, must be considered in pressure-driven, CFF-based DF. Since most of all referred CFF studies employed membrane MWCOs of 100 kDa or higher to keep the processing time within limits, we additionally included a 10 kDa MWCO, which is commonly used for dialysis, alongside the 100 kDa MWCO membrane to provide a comparative perspective. The authors decided on a constant TMP enabled through an automatic valve on the retentate side for the CFF runs with the 10 kDa MWCO membrane. In comparison, a capillary on the permeate side led to a constant permeate back pressure for the runs using the 100 kDa MWCO membrane. Comprehensive parameter studies considering membrane-related next to operational parameter variations in constant-volume DF have not been reported within the broader category of lipid-based particles.

Specifically, those lipid-based particles may be sensitive to applied pressures and specific types of pumps, valves, membrane material, or membrane format, as each of these factors can generate its shear rate, leading to various shear forces that could further affect the particle characteristics. The selected membrane materials mPES and mRC exhibit a hydrophilic nature, facilitating water permeability and preventing fouling [14]. Regardless of the membrane material, comparable lipid recoveries of approximately 86% to 89% were achieved, significantly surpassing the reported 73% recovery for LNP purification by CFF [17] and closely aligning with studies on liposome purification by CFF [19,22,32]. Comparable lipid recoveries stand in contrast to the differently pronounced permeability drops observed throughout the different CFF runs, which typically indicate fouling behavior. Overall, optimizing surface areas or processing larger volumes can help reduce product accumulation on the membrane, thereby enhancing overall recovery.

Besides potential interactions, membrane-related and operational parameters may influence the target product. Our strategy to include monitoring tools aligns with the PAT initiative [21], as at-line measurements provide near real-time process insights. To the best of the authors' knowledge, we are the first to have implemented at-line DLS enabling tracking of the LNP particle size and size distribution throughout CFF-based processing, resolving characteristic changes from DV to DV. Among lipid-based particles, Forbes et al. [22] claimed at-line monitoring of liposome particle size but focused on in-process monitoring between process steps rather than on time- or DV-resolved insights into CFF using CFF intermediates. DLS would also be suitable for on-line implementation using a suitable flow cell, but this has not yet been reported for LNPs. An advancement has led to spatially resolved DLS, which has already been applied to turbid nanoemulsions [34] and liposomes purified by single-pass CFF [18]. Sheybanifard et al. [18] not only monitored the product but also employed in-line near-infrared spectroscopy to quantify residual ethanol, which could similarly be applied to monitor ethanol depletion over constant-volume DF and UF.

4.3. Effects of cross-flow filtration-based purification on lipid nanoparticles

Despite being a time- and resource-efficient purification procedure, CFF is rarely reported for LNPs, and even less frequently are the UF/DF process dynamics examined through a holistic analysis of CFF intermediates. Given the limited research on CFF intermediates in CFF-based LNP purification, the following summarizes the key findings and their implications.

We found a time-dependent size increase of LNPs, which seems independent of selected processing parameters. So far, the LNP size increase over CFF-based DF has been merely described by Geng et al. [15]. They examined a DF process for three different LNP formulations and observed a stabilized LNP size after two DV for all three formulations. After two DV, approximately 87% of the initial buffer and ethanol are expected to be removed, assuming unrestricted membrane permeability for smaller molecules [14].

Moreover, Geng et al. [15] observed differences in the way of particle fusion depending on the purification procedure, as the initial absence of ethanol led to more homogeneous particles than its initial presence during DF to physiological pH, but clearly stated that the fusion is pH-driven. Fusion behavior is also observed to be pH-dependent during dialysis [10] and is hypothesized to depend on the ionizable lipid and its pKa [8]. Although DOTAP is a pH-insensitive, permanent cationic lipid, changes in the amount of positive charge seem to affect LNP fusion behavior. In particular, the PEG lipid plays a key role in the colloidal stability and fusion behavior of LNPs. The molar content of the PEG lipid affects particle size and defines its equilibrium size, which also depends on the pH of the solution [35,36]. Overall, the size increase of LNPs may be linked to the PEG-dependent equilibrium size and the presence

of a cationic lipid, combined with a pH increase throughout the process. Studies on CFF-based DF processes of liposomes have shown no particle size increase [22,32], which might be attributed to the structural differences between LNP and liposomes. Another factor that might have influenced this outcome is the process condition applied in those studies, where ethanol was solely removed without increasing the pH or altering the buffer [22,32]. Others observed similar behavior of cationic liposomes performing discontinuous DF with DF cycles consisting of concentration and manual dilution [19].

Since the observed size increase during our DF/UF processes is closely linked to the processing time of LNPs, the potential influence of shear forces must be considered. The time-dependent LNP size increase indicates that the pump-induced shear rate has more impact on particle size than the membrane-induced shear rates. This conclusion is drawn from the fact that the membrane-induced shear rates are format-dependent, while the pump-induced shear rates were constant across all experiments. Thus, the time-dependent increase in LNP size can be attributed to the pump cycles, which correspond to the processing time. To reduce processing time, single-pass CFF may offer an effective strategy for LNP purification. Here, too, liposome studies have shown no size increase of their PEGylated liposomes during continuous processing by single-pass CFF [18] or during continuous, in-line single-pass DF using such serially connected filter membranes [33].

Besides the observed size increase across CFF-based LNP purification, an increase in size was also observed in the individual CFF intermediates over the storage time, which contrasts with the observed size deviations seen from at-line to off-line (day 1) of later CFF intermediates. The observed deviations between at-line and off-line DLS measurements could be assigned to two overlapping phenomena. A systematic, method-derived offset upwards in size for at-line DLS for all CFF intermediates may co-occur with the tendency of enhanced size increase of early CFF intermediates compared to later CFF intermediates. The latter tendency can be observed across 14 days of storage.

LNP size was the only measured particle characteristic that changed during storage. All LNPs exhibited a size increase, with the most pronounced growth in early CFF intermediates and dialyzed LNPs, which initially measured half the size of the final CFF-purified LNPs. Storage-related size increase for dialyzed LNPs with an identical lipid molar ratio and cargo has already been shown in our previous work [24]. Although PEG-lipid content plays a crucial role in preventing fusion, final DF/UF-purified LNPs exhibit less fusion than dialyzed LNPs, even though the PEG content is identical, suggesting that storage-induced fusion behavior may be independent of PEG-lipid concentration. Storage-related size increase of LNP purification intermediates and after CFF-based purification was so far only observed by Geng et al. [15]. Their final DF-purified LNPs after eight DV showed a size increase of 6.1 nm over a 2-month storage. Due to the different LNP sizes of the starting material, overall processing time, and DV, absolute size comparisons were omitted. Our DF processes for six DV had comparable or higher process times and hence resulted in different sizes after DF due to the found time dependency. Exemplarily, DF time in the mRC-100 CFF process was comparable to the DF process presented by Geng et al. [15], leading to a size increase of 2.1 nm over two weeks of storage. Overall, storage-induced size increases of CFF intermediates appear comparable across the CFF runs. For further concentrated LNPs by UF following DF, storage stability data has not been reported in the literature.

Many studies have highlighted the importance of production parameters during microfluidic mixing [7,8,5] when controlling LNP characteristics such as size. However, Vargas et al. [9] has also found that those identified correlations change through subsequent dialysis, emphasizing the consideration of dialysis or any other treatment or purification step. On-chip dilution has been introduced as a size-controlled treatment strategy [13], which still had to undergo a purification step. In this context, LNP purification by CFF is far too little explored and reported in the literature. With the observed time-dependent increase in particle size, the authors state that CFF might be the purification process for targeted, size-controlled LNPs. However, this is why several questions in this study still require further investigation. The question arises about how far the LNPs are from their equilibrium size. Our observations that dialyzed LNPs increased in size over storage to a greater extent than CFF-purified LNPs may indicate CFF as a representable purification method to achieve the equilibrium size faster. Additionally, modifications in CFF design, such as extending the processing time, might enable the LNPs to reach equilibrium size. The influence of pump-induced shear rates on the size increase of LNPs remains a key consideration, and since shear-sensitive pumps are now available on the market, a comparative study would be interesting. Furthermore, the emergence of a second larger LNP population raises the question of what triggers this behavior and whether it could indicate particle instability, making an investigation into the formation and morphology of such particles urgently required. Progress toward optimizing filtration performance can only be made after reassessing and clarifying these questions related to controlling the target LNP characteristics. In the future, an investigation into various operating conditions, membranes, and advanced membrane technologies, along with their associated shear forces and fouling behavior, may be undertaken.

4.4. Effects of sterile filtration on lipid nanoparticles purified by cross-flow filtration

Although sterile filtration is a crucial step in biopharmaceutical manufacturing, it is often seen as problematic regarding nanoparticle therapeutics due to the similarity between nanoparticle size and filter pore size. Besides filtration capacity, nanoparticle characteristics and their recovery are essential parameters for evaluation.

Sterile filtration of the CFF-purified LNPs led to significant changes in the intensity-weighted size distributions but resulted only in a minor reduction in Z-average. According to the size distribution and contrary to our expectations, LNPs larger than the 0.22 µm pore size were still found in the filtrate. Due to a lack of literature describing this phenomenon, the authors propose several hypotheses. One possibility may be that LNPs undergo deformation into a more elliptical or oval shape due to filtration forces, allowing them to pass through the filter pores. Literature on nanoparticle deformability is relatively rare, but Hirsjärvi et al. [16] found same-sized hybrid polymer-lipid particles in the CFF filtrate, even though their particle size exceeded the evaluated MWCO. Conversely, the increased intensity of particles between the two most pronounced populations suggests simultaneous fragmentation and hence formation of intermediate-sized particles, which may be due to experienced shear forces during filtration. However, those hypotheses could not be evaluated in this study. It has to be noted that the hydrodynamic diameter assessed encompasses the hydration shell of the particle, which is the underlying principle of the DLS measurement.

In contrast to our findings, no substantial change in the particle size and size distribution was observed in the sterile filtration study of Messerian et al. [37] with similar-sized LNPs. Further, our lipid recoveries ranged between 72% and 96%, with 96% being close to those reported lipid recoveries. Messerian et al. [37] examined the effects of different pressures on filtration and found deposits on the membrane, which were further analyzed in-depth by Messerian et al. [38]. They observed an amorphous 100 nm-thick deposit on the surface of a 0.2 µm polyethersulfone filter, suggesting that it may form due to a combination of size-based retention, adsorption, filtration forces, and LNP coalescence. Adsorption is based on material-product interactions, and given that LNP surfaces exhibit a broad range of functional groups, physical or chemical interactions may occur. The adhesion forces of hydrophobic functional groups on the filter could be evaluated using the method described by Wang et al. [39], who utilized atomic force microscopy to study the interactions between hydrophilic functional groups and LNPs.

Compared to filtration studies under desired pressures [37,38], we performed sterile filtration by hand, which could be linked to variations in recovery. Further, a concentration dependence is evident, as higher

recoveries were observed for the dialyzed LNPs compared to pre-diluted, dialyzed LNP. In general, adjusting the process volume, LNP concentration, or filter area could further contribute to optimizing recovery. For high lipid concentrations, sterile filtration of purified PEGylated liposomes has been reported to achieve recoveries of up to 100% [33].

In summary, sterile filtration affected LNP size distribution but did not erase populations larger than or around 200 nm completely, possibly due to shear-induced deformation or fragmentation of LNPs.

5. Conclusion

In conclusion, we present a CFF parameter study for LNP purification by DF/UF, investigating the impact of CFF-based processing on process performance and particle characteristics.

A series of dialysis experiments revealed that pre-dilution of LNPs with synthesis buffer as a pretreatment procedure allows for reducing the ethanol content prior CFF-based purification without affecting the LNP characteristics. Time- and resource-efficient buffer exchange and product concentration were addressed by constant-volume DF mode over six DV followed by LNP concentration by UF. Although the systematic strategy varying either the membrane characteristics material, format, and area, or the membrane MWCO and the system pressure setting has been introduced to investigate their parameter impact on particle characteristics, a contrary dependency was found—a processing time-dependent particle size increase. With the novel aspect aiming for near real-time monitoring by implementing at-line DLS measurements, time-resolved insights into changes in particle size and size distribution were provided. A noticeable trend was observed in particle size increases during storage, with an enhanced size increase of dialyzed LNPs and early CFF intermediates compared to later CFF intermediates and final CFF-purified LNPs, leading to several hypotheses for the underlying reason, including the equilibrium size of LNPs. Sterile filtration of purified LNPs again introduced changes in the particle size and size distribution, suggesting shear-induced particle deformation and fragmentation.

Overall, this parameter study, combined with at-line and off-line analytics yielding intensified process insights, provides a solid foundation for future investigations into the formation behavior and morphology changes by CFF-based LNP processing, hence paving the way for future CFF applications for size-controlled LNP purification.

CRediT authorship contribution statement

Annabelle Dietrich: Writing – review & editing, Writing – original draft, Visualization, Validation, Software, Methodology, Investigation, Formal analysis, Data curation, Conceptualization. **Nicole Beckert:** Writing – review & editing, Writing – original draft, Visualization, Validation, Software, Methodology, Investigation, Formal analysis, Data curation, Conceptualization. **Jürgen Hubbuch:** Writing – review & editing, Supervision, Funding acquisition, Conceptualization.

Funding

This research project received funding from the ECSEL Joint Undertaking (JU) under grant agreement No. 876190. The JU receives support from the European Union's Horizon 2020 research and innovation programme and the Netherlands, Italy, Ireland, Spain, Belgium, Finland, Germany, Austria, Portugal, Hungary, Romania, and Switzerland.

Declaration of competing interest

All authors declare that they have no known competing financial interests or personal relationships that could have appeared to influence the work reported in this paper.

Acknowledgements

We express our gratitude for the support provided by the KIT Publication Fund of the Karlsruhe Institute of Technology. We also extend our heartfelt thanks to Lipoid (Ludwigshafen) for their generous donation of phospholipids for this research. Additionally, we sincerely appreciate Luise Appoldt's essential contribution to this project through her experimental work.

Appendix. Supplementary material

Supplementary material related to this article can be found online at https://doi.org/10.1016/j.jcis.2025.137663.

Data availability

Data will be made available on request.

References

[1] P.R. Cullis, P.L. Felgner, The 60-year evolution of lipid nanoparticles for nucleic acid delivery, Nat. Rev. Drug Discov. 23 (2024) 709–722, https://doi.org/10.1038/s41573-024-00977-6.

[2] I. Urits, D. Swanson, M.C. Swett, A. Patel, K. Berardino, A. Amgalan, A.A. Berger, H. Kassem, A.D. Kaye, O. Viswanath, A review of patisiran (onpattro®) for the treatment of polyneuropathy in people with hereditary transthyretin amyloidosis, Neurol. Ther. 9 (2020) 301–315, https://doi.org/10.1007/s40120-020-00208-1.

[3] C.H. Albertsen, J.A. Kulkarni, D. Witzigmann, M. Lind, K. Petersson, J.B. Simonsen, The role of lipid components in lipid nanoparticles for vaccines and gene therapy, Adv. Drug Deliv. Rev. 188 (2022) 114416, https://doi.org/10.1016/j.addr.2022.114416.

[4] Y. Fan, C.W. Yen, H.C. Lin, W. Hou, A. Estevez, A. Sarode, A. Goyon, J. Bian, J. Lin, S.G. Koenig, D. Leung, K. Nagapudi, K. Zhang, Automated high-throughput preparation and characterization of oligonucleotide-loaded lipid nanoparticles, Int. J. Pharm. 599 (2021) 120392, https://doi.org/10.1016/j.ijpharm.2021.120392.

[5] K. Okuda, Y. Sato, K. Iwakawa, K. Sasaki, N. Okabe, M. Maeki, M. Tokeshi, H. Harashima, On the size-regulation of rna-loaded lipid nanoparticles synthesized by microfluidic device, J. Control. Release 348 (2022) 648–659, https://doi.org/10.1016/j.jconrel.2022.06.017.

[6] M.J.W. Evers, J.A. Kulkarni, R. van der Meel, P.R. Cullis, P. Vader, R.M. Schiffelers, State-of-the-art design and rapid-mixing production techniques of lipid nanoparticles for nucleic acid delivery, Small Methods 2 (2018) 1700375, https://doi.org/10.1002/smtd.201700375.

[7] C.B. Roces, G. Lou, N. Jain, S. Abraham, A. Thomas, G.W. Halbert, Y. Perrie, Manufacturing considerations for the development of lipid nanoparticles using microfluidics, Pharmaceutics 12 (2020) 1095, https://doi.org/10.3390/pharmaceutics12111095.

[8] T. Terada, J.A. Kulkarni, A. Huynh, S. Chen, R. van der Meel, Y.Y.C. Tam, P.R. Cullis, Characterization of lipid nanoparticles containing ionizable cationic lipids using design-of-experiments approach, Langmuir 37 (2021) 1120–1128, https://doi.org/10.1021/acs.langmuir.0c03039.

[9] R. Vargas, M. Romero, T. Berasategui, D.A. Narváez-Narváez, P. Ramirez, A. Nardi-Ricart, E. García-Montoya, P. Pérez-Lozano, J.M. Suñe-Negre, C. Moreno-Castro, C. Hernández-Munain, C. Suñe, M. Suñe-Pou, Dialysis is a key factor modulating interactions between critical process parameters during the microfluidic preparation of lipid nanoparticles, Colloids Interface Sci. Commun. 54 (2023), https://doi.org/10.1016/j.colcom.2023.100709.

[10] J.A. Kulkarni, D. Witzigmann, J. Leung, Y.Y.C. Tam, P.R. Cullis, On the role of helper lipids in lipid nanoparticle formulations of siRNA, Nanoscale 11 (2019) 21733–21739, https://doi.org/10.1039/c9nr09347h.

[11] L.B. Jeffs, L.R. Palmer, E.G. Ambegia, C. Giesbrecht, S. Ewanick, I. MacLachlan, A scalable, extrusion-free method for efficient liposomal encapsulation of plasmid DNA, Pharm. Res. 22 (2005) 362–372, https://doi.org/10.1007/s11095-004-1873-z.

[12] R. Mihaila, S. Chang, A.T. Wei, Z.Y. Hu, D. Ruhela, T.R. Shadel, S. Duenwald, E. Payson, J.J. Cunningham, N. Kuklin, D.J. Mathre, Lipid nanoparticle purification by Spin Centrifugation-Dialysis (SCD): a facile and high-throughput approach for small scale preparation of siRNA-lipid complexes, Int. J. Pharm. 420 (2011) 118–121, https://doi.org/10.1016/j.ijpharm.2011.08.017.

[13] N. Kimura, M. Maeki, Y. Sato, A. Ishida, H. Tani, H. Harashima, M. Tokeshi, Development of a microfluidic-based post-treatment process for size-controlled lipid nanoparticles and application to siRNA delivery, ACS Appl. Mater. Interfaces 12 (2020) 34011–34020, https://doi.org/10.1021/acsami.0c05489.

[14] R. van Reis, A. Zydney, Bioprocess membrane technology, J. Membr. Sci. 297 (2007) 16–50, https://doi.org/10.1016/j.memsci.2007.02.045.

[15] C. Geng, K. Zhou, Y. Yan, C. Li, B. Ni, J. Liu, Y. Wang, X. Zhang, D. Wang, L. Lv, Y. Zhou, A. Feng, Y. Wang, C. Li, A preparation method for mRNA-LNPs with improved properties, J. Control. Release 364 (2023) 632–643, https://doi.org/10.1016/j.jconrel.2023.11.017.

[16] S. Hirsjärvi, G. Bastiat, P. Saulnier, J.P. Benoît, Evaluation of surface deformability of lipid nanocapsules by drop tensiometer technique, and its experimental assessment by dialysis and tangential flow filtration, Int. J. Pharm. 434 (2012) 460–467, https://doi.org/10.1016/j.ijpharm.2012.06.019.

[17] Y. Sakurai, T. Hada, H. Harashima, Scalable preparation of poly(ethylene glycol)-grafted siRNA-loaded lipid nanoparticles using a commercially available fluidic device and tangential flow filtration, J. Biomater. Sci. Polym. Ed. 28 (2017) 1086–1096, https://doi.org/10.1080/09205063.2017.1291297.

[18] M. Sheybanifard, L.P. Guerzoni, A. Omidinia-Anarkoli, L. De Laporte, J. Buyel, R. Besseling, M. Damen, A. Gerich, T. Lammers, J.M. Metselaar, Liposome manufacturing under continuous flow conditions: towards a fully integrated set-up with in-line control of critical quality attributes, Lab Chip 23 (2022) 182–194, https://doi.org/10.1039/d2lc00463a.

[19] N. Dimov, E. Kastner, M. Hussain, Y. Perrie, N. Szita, Formation and purification of tailored liposomes for drug delivery using a module-based micro continuous-flow system, Sci. Rep. 7 (2017), https://doi.org/10.1038/s41598-017-11533-1.

[20] R.D. Worsham, V. Thomas, S.S. Farid, Impact of ethanol on continuous inline diafiltration of liposomal drug products, Biotechnol. J. 18 (2023) 1–9, https://doi.org/10.1002/biot.202300194.

[21] FDA, Guidance for Industry: PAT—a framework for innovative pharmaceutical development, manufacturing, and quality assurance, Technical Report, 2004.

[22] N. Forbes, M.T. Hussain, M.L. Briuglia, D.P. Edwards, J.H. Horst, N. Szita, Y. Perrie, Rapid and scale-independent microfluidic manufacture of liposomes entrapping protein incorporating in-line purification and at-line size monitoring, Int. J. Pharm. 556 (2019) 68–81, https://doi.org/10.1016/j.ijpharm.2018.11.060.

[23] M. Rüdt, T. Briskot, J. Hubbuch, Advances in downstream processing of biologics – spectroscopy: an emerging process analytical technology, J. Chromatogr. A 1490 (2017) 2–9, https://doi.org/10.1016/j.chroma.2016.11.010.

[24] N. Beckert, A. Dietrich, J. Hubbuch, RP-CAD for lipid quantification: systematic method development and intensified LNP process characterization, Pharmaceuticals 17 (2024), https://doi.org/10.3390/ph17091217.

[25] T. McIntosh, R. McDaniel, S. Simon, Induction of an interdigitated gel phase in fully hydrated phosphatidylcholine bilayers, Biochim. Biophys. Acta, Biomembr. 731 (1983) 109–114, https://doi.org/10.1016/0005-2736(83)90403-0.

[26] F.W. Stetter, T. Hugel, The nanomechanical properties of lipid membranes are significantly influenced by the presence of ethanol, Biophys. J. 104 (2013) 1049–1055, https://doi.org/10.1016/j.bpj.2013.01.021.

[27] J. Paxman, B. Hunt, D. Hallan, S.R. Zarbock, D.J. Woodbury, Drunken membranes: short-chain alcohols alter fusion of liposomes to planar lipid bilayers, Biophys. J. 112 (2017) 121–132, https://doi.org/10.1016/j.bpj.2016.11.3205.

[28] A. Hardianto, Z.S. Muscifa, W. Widayat, M. Yusuf, T. Subroto, The effect of ethanol on lipid nanoparticle stabilization from a molecular dynamics simulation perspective, Molecules 28 (2023), https://doi.org/10.3390/molecules28124836.

[29] K.J. Hassett, J. Higgins, A. Woods, B. Levy, Y. Xia, C.J. Hsiao, E. Acosta, Örn Almarsson, M.J. Moore, L.A. Brito, Impact of lipid nanoparticle size on mrna vaccine immunogenicity, J. Control. Release 335 (2021) 237–246, https://doi.org/10.1016/j.jconrel.2021.05.021.

[30] A. Pittiu, M. Pannuzzo, L. Casula, R. Pireddu, D. Valenti, M.C. Cardia, F. Lai, A. Rosa, C. Sinico, M. Schlich, Production of liposomes by microfluidics: the impact of post-manufacturing dilution on drug encapsulation and lipid loss, Int. J. Pharm. 664 (2024) 124641, https://doi.org/10.1016/j.ijpharm.2024.124641.

[31] Y. Perrie, C. Webb, S. Khadke, S.T. Schmidt, C.B. Roces, N. Forbes, G. Berrie, The impact of solvent selection: strategies to guide the manufacturing of liposomes using microfluidics, Pharmaceutics 11 (2019), https://doi.org/10.3390/pharmaceutics11120653.

[32] C. Webb, N. Forbes, C.B. Roces, G. Anderluzzi, G. Lou, S. Abraham, L. Ingalls, K. Marshall, T.J. Leaver, J.A. Watts, J.W. Aylott, Y. Perrie, Using microfluidics for scalable manufacturing of nanomedicines from bench to GMP: a case study using protein-loaded liposomes, Int. J. Pharm. 582 (2020) 119266, https://doi.org/10.1016/j.ijpharm.2020.119266.

[33] C.B. Roces, E.C. Port, N.N. Daskalakis, J.A. Watts, J.W. Aylott, G.W. Halbert, Y. Perrie, Rapid scale-up and production of active-loaded PEGylated liposomes, Int. J. Pharm. 586 (2020) 119566, https://doi.org/10.1016/j.ijpharm.2020.119566.

[34] R. Besseling, M. Damen, J. Wijgergangs, M. Hermes, G. Wynia, A. Gerich, New unique PAT method and instrument for real-time inline size characterization of concentrated, flowing nanosuspensions, Eur. J. Pharm. Sci. 133 (2019) 205–213, https://doi.org/10.1016/j.ejps.2019.03.024.

[35] J.A. Kulkarni, M.M. Darjuan, J.E. Mercer, S. Chen, R. van der Meel, J.L. Thewalt, Y.Y.C. Tam, P.R. Cullis, On the formation and morphology of lipid nanoparticles containing ionizable cationic lipids and sirna, ACS Nano 12 (2018) 4787–4795, https://doi.org/10.1021/acsnano.8b01516.

[36] J.A. Kulkarni, D. Witzigmann, J. Leung, R. van der Meel, J. Zaifman, M.M. Darjuan, H.M. Grisch-Chan, B. Thöny, Y.Y.C. Tam, P.R. Cullis, Fusion-dependent formation of lipid nanoparticles containing macromolecular payloads, Nanoscale 11 (2019) 9023–9031, https://doi.org/10.1039/C9NR02004G.

[37] K.O. Messerian, A. Zverev, J.F. Kramarczyk, A.L. Zydney, Pressure-dependent fouling behavior during sterile filtration of mrna-containing lipid nanoparticles, Biotechnol. Bioeng. 119 (2022) 3221–3229, https://doi.org/10.1002/bit.28200.

[38] K.O. Messerian, A. Zverev, J.F. Kramarczyk, A.L. Zydney, Characterization and associated pressure-dependent behavior of deposits formed during sterile filtration of mrna-lipid nanoparticles, J. Membr. Sci. 684 (2023) 121896, https://doi.org/10.1016/j.memsci.2023.121896.

[39] J. Wang, J. Zhang, S. Li, H. Qian, D. Liu, I. Prado, S. Wang, A. Bhambhani, H. Zeng, Probing the interaction mechanisms of lipid nanoparticle-encapsulated mrna with surfaces of diverse functional groups: implication for mrna transport, Chem. Eng. Sci. 301 (2025) 120693, https://doi.org/10.1016/j.ces.2024.120693.